Direction-of-Arrival Estimation Exploiting Oversampled Uniform Linear Arrays

Md. Waqeeb T. S. Chowdhury, *Student Member, IEEE*, and Yimin D. Zhang, *Fellow, IEEE*

***Abstract*—This letter investigates the impact of spatially oversampling a uniform linear array (ULA) on its identifiability. Under perfect statistical and noise-free conditions, the rank of the array covariance matrix is identical to that of the array manifold. We analyze the Wronskian of the steering vector components in the oversampled array manifold and demonstrate that the array manifold maintains full theoretical rank, but the Wronskian tends to vanish as the interelement spacing decreases. To evaluate the practical degrees-of-freedom (DOFs) of the oversampled array, we further examine the numerical rank of the manifold matrix by analyzing an upper bound of the minimum singular value and its dependence on the number of sensors and the oversampling factor. This analysis reveals the conditions under which the minimum singular value falls below a given threshold, causing a loss of numerical rank and correspondingly its DOFs in the oversampled array. Our results indicate that, as the number of sensors in the ULA increases within a fixed aperture, the incremental gain in numerical rank from oversampling progressively diminishes.**

***Index Terms*—Direction-of-arrival estimation, spatial oversampling, Wronskian, smallest singular value, identifiability analysis.**

I. Introduction

DIRECTION-of-arrival (DOA) estimation is a key technique in array signal processing with broad applications in radar, sonar, and wireless communications [1]–[7]. Uniform linear arrays (ULAs) are typically designed with half-wavelength interelement spacing to meet the spatial Nyquist criterion. As a result, an N-element ULA resolves up to $N-1$ signals. On the other hand, non-integer arrays with sensors off the half-wavelength integer grid, offer greater design flexibility [8], [9]. In particularly, spatially oversampled arrays with spacing smaller than half-wavelength can accommodate more sensors within the same aperture compared to integer-spaced ULAs. On the other hand, multi-frequency arrays utilize mutually coprime frequencies to significantly increase the number of degrees of freedom (DOFs) [10]–[13]. This concept was generalized to the rational domain in [14], [15] such that virtual sensor locations at non-integer multiples of the half-wavelength are used to allow greater flexibility in array and frequency design.

These emerging developments motivate us to explore the relationship between spatial oversampling using interelement spacing below half-wavelength and the resulting DOFs. In our previous works [16], [17], we analyzed the effects of reducing the interelement spacing of a ULA on the number of DOFs and introduced a method to identify the threshold at which an N-element ULA loses a DOF. While these analyses sheds lights on the condition for a compressed ULA to lose a DOF, they leave open a fundamental and less explored question: Given a fixed aperture, can we increase the number of DOFs by placing more sensors?

It is well known that oversampling band-limited signals beyond the Nyquist rate does not provide additional information. However, a key distinction in the context of oversampled array lies in that the array aperture is finite. As a result, the array data are not spatially band-limited, thus allowing additional sensors placed closer than half-wavelength Nyquist spacing to contribute additional DOFs. Motivated by this observation, we analyze the enhanced identifiability of oversampled sensor arrays. More specifically, under ideal statistical and noise-free conditions, we reveal that the additional sensors introduced through spatial oversampling contribute to the theoretical rank of the array manifold. However, as the oversampling factor or number of sensors in the ULA increases, the smallest singular value of the array manifold becomes infinitesimally small. When it falls below a certain threshold, it can be considered negligible for practical applications. As a result, the oversampled array loses its numerical rank, and its effective DOFs fall below the number of sensors. In this context, the effective numerical rank is evaluated by analyzing the smallest singular value and determining when it drops below a critical threshold. In the limit of an infinitely large array, oversampling no longer increases the numerical rank of the array manifold, indicating that its contribution becomes negligible. We provide mathematical analyses to support these observations and validate our findings through numerical examples.

A related but distinct concept is holographic multiple-input multiple-output (MIMO) systems in the context of next-generation wireless networks. These system utilize highly oversampled antenna arrays and programmable meta-materials to enable continuous aperture processing and enhanced spatial multiplexing [18]–[21]. However, most studies focus on their capability to transform the wireless environment in a programmable manner to enhance communication and localization capabilities, they do not comprehensively address the impact of reduced interelement spacing on array identifiability.

Notations: We use lower-case (upper-case) bold letters to denote vectors (matrices). In particular, $\mathbf{I}_N$ stands for an $N\times N$ identity matrix, and $\mathbf{0}$ indicates a zero vector or matrix of appropriate dimension. $\otimes$, $(\cdot)^{\mathrm{T}}$ and $(\cdot)^{\mathrm{H}}$ respectively indicate the convolution operation, the transpose and Hermitian of a matrix or a vector and the symbol $\jmath=\sqrt{-1}$ represents the unit imaginary number. The determinant of a square matrix $\mathbf{B}$ is given by $|\mathbf{B}|$. The kth derivative of a function $f(x)$ is denoted

This work was supported in part by the National Science Foundation (NSF) under Grant ECCS-2236023 and in part by the Air Force Office of Scientific Research (AFOSR) under Grant FA9550-23-1-0255.

The authors are with the Department of Electrical and Computer Engineering, Temple University, Philadelphia, PA 19122, USA (emails: waqeebsayeed@temple.edu, ydzhang@temple.edu).

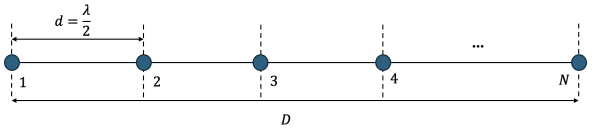

(a) N-element ULA with half-wavelength spacing d

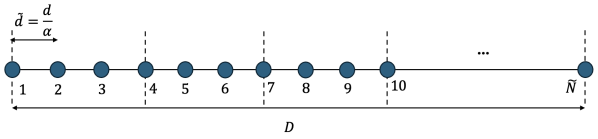

(b) $\tilde{N}$-element oversampled ULA with compressed spacing $\tilde{d}$

Fig. 1: An N-element ULA with half-wavelength spacing is oversampled by a factor of $\alpha = 3$ keeping aperture fixed.

by $f^{(k)}(x)$. Finally, $\mathbb{E}(\cdot)$ denotes the statistical expectation and diag$(\cdot)$ represent the construction of a diagonal matrix.

II. Signal Model

The baseline scenario assumes an N-element ULA with interelement spacing $d = \lambda/2$, where λ denotes the signal wavelength. When L uncorrelated signals impinge on the array with distinct DOAs $\theta_1, \theta_2, \cdots, \theta_L$, the received baseband signal vector is given as

$$\mathbf{x}(t) = \sum_{l=1}^{L} \mathbf{a}(\theta_l) s_l(t) + \mathbf{n}(t) = \mathbf{A}\mathbf{s}(t) + \mathbf{n}(t), \tag{1}$$

where

$$\mathbf{a}(\theta_l) = [e^{\jmath p_1 \phi_l}, e^{\jmath p_2 \phi_l}, \cdots, e^{\jmath p_N \phi_l}]^{\mathrm{T}} \tag{2}$$

is the steering vector of the array corresponding to the lth signal $s_l(t)$ with $\phi_l = (2\pi d/\lambda)\sin(\theta_l)$ for $l \in [1, 2, \cdots, L]$, and $p_n = n - 1$ for $n \in [1, 2, \cdots, N]$ is the sensor location index of the nth sensor. The array manifold is given as $\mathbf{A} = [\mathbf{a}(\theta_1), \mathbf{a}(\theta_2), \cdots, \mathbf{a}(\theta_L)] \in \mathbb{C}^{N \times L}$. We denote $\mathbf{s}(t) = [s_1(t), s_2(t), \cdots, s_L(t)]^{\mathrm{T}}$ and assume that all signals are zero mean and mutually uncorrelated. Furthermore, $\mathbf{n}(t) \sim \mathcal{CN}(\mathbf{0}, \sigma_n^2 \mathbf{I}_N)$ stands for the additive circularly complex white Gaussian noise vector. The covariance matrix of the received vector assuming perfect statistics is expressed as

$$\mathbf{R}_{\mathbf{x}} = \mathbb{E}[\mathbf{x}(t)\mathbf{x}^{\mathrm{H}}(t)] = \mathbf{A}\mathbf{R}_{\mathbf{s}}\mathbf{A}^{\mathrm{H}} + \sigma_n^2 \mathbf{I}_N, \tag{3}$$

where $\mathbf{R}_{\mathbf{s}} = \mathbb{E}[\mathbf{s}(t)\mathbf{s}^{\mathrm{H}}(t)] = \mathrm{diag}([\sigma_1^2, \sigma_2^2, \cdots, \sigma_L^2]) \in \mathbb{C}^{L \times L}$ is the signal covariance matrix. Performing eigen-decomposition on $\mathbf{R}_{\mathbf{x}}$ yields

$$\mathbf{R}_{\mathbf{x}} = \sum_{n=1}^{N} \gamma_n \mathbf{u}_n \mathbf{u}_n^{\mathrm{H}}, \tag{4}$$

where γ_n and $\mathbf{u}_n$ denote the nth eigenvalue and the corresponding eigenvector, respectively. Ordering the eigenvalues in descending manner, the relationship among eigenvalues is given as $\gamma_1 \geq \gamma_2 \geq \cdots \geq \gamma_L > \gamma_{L+1} = \cdots = \gamma_N = \sigma_n^2$.

In noise-free scenario, i.e., $\sigma_n^2 = 0$, the smallest $N - L$ eigenvalues reduce to zero, i.e., $\gamma_{L+1} = \gamma_{L+2} = \cdots = \gamma_N = 0$. To fully comprehend the effects of the array structure on the rank of the covariance matrix corresponding the impinging signals, we consider noise-free conditions so that $\mathrm{rank}(\mathbf{R}_{\mathbf{x}}) = \mathrm{rank}(\mathbf{A})$.

III. Spatial Oversampling and Its Effect on the Array Manifold Rank

This section examines how the theoretical and numerical ranks of the array manifold vary with the oversampling factor $\alpha > 1$ while keeping the ULA aperture fixed. The baseline ULA consists of N elements with half-wavelength spacing, i.e., $d = \lambda/2$, and the array aperture is $D = (N-1)d$. For a spatially oversampled ULA with oversampling factor α, its interelement spacing is $\tilde{d} = d/\alpha$, and $\tilde{N} = \alpha(N-1) + 1$ sensors exactly span the same array aperture.

In Subsection III-A, we assess the impact of increasing N and α on the linear independence of the steering vector elements, demonstrating that the oversampled array manifold remains theoretically full rank. Subsection III-B examines the relationship of the smallest singular value $\mu_{\min}$ of the oversampled array manifold with α and N, offering insights into when the array manifold becomes numerically rank deficient as $\mu_{\min}$ falls below the threshold. In this subsection, we assume that the number of signals is equal to the number of sensors, and that the sine of their DOAs are uniformly distributed over the full angular field of view of the linear array. This setup ensures that any reduction in the DOFs arises solely from the array configuration.

A. Theoretical Rank of Oversampled Array Manifold

The steering vector of the oversampled ULA corresponding to the lth signal is

$$\tilde{\mathbf{a}}(\theta_l) = [e^{\jmath p_1 \tilde{\phi}_l}, e^{\jmath p_2 \tilde{\phi}_l}, \cdots, e^{\jmath p_{\tilde{N}} \tilde{\phi}_l}]^{\mathrm{T}}, \tag{5}$$

where $\tilde{\phi}_l = (2\pi\tilde{d}/\lambda)\sin(\theta_l)$, and the corresponding array manifold is given as $\tilde{\mathbf{A}} = [\tilde{\mathbf{a}}(\theta_1), \tilde{\mathbf{a}}(\theta_2), \cdots, \tilde{\mathbf{a}}(\theta_L)] \in \mathbb{C}^{\tilde{N} \times L}$. Figs. 1(a) and 1(b) respectively show an N-element baseline ULA and an $\tilde{N}$-element oversampled ULA with $\alpha = 3$. For the baseline ULA depicted in Fig. 1(a), the maximum rank of the array manifold $\mathbf{A}$ is N. We are interested in the maximum rank of the oversampled ULA in Fig. 1(b). Note that, for some $\tilde{\mathbf{A}}$, if $\max\ \mathrm{rank}(\tilde{\mathbf{A}}) > \max\ \mathrm{rank}(\mathbf{A}) = N$, it implies that, compared to the baseline ULA, additional DOFs can be achieved by adding sensors in the oversampled ULA while the array aperture remains the same.

Lemma 1: The array manifold of the oversampled ULA, $\tilde{\mathbf{A}}$ is always theoretically full rank irrespective of the number of sensors N and the oversampling factor α.

Proof. For any K functions $f_1(x)$, $f_2(x)$, $\cdots$, $f_K(x)$ that are at least $K-1$ times differentiable, the Wronskian is given as

$$W_f(x) = \begin{vmatrix} f_1(x) & f_2(x) & \cdots & f_K(x) \\ f_1^{(1)}(x) & f_2^{(1)}(x) & \cdots & f_K^{(1)}(x) \\ \vdots & \vdots & \ddots & \vdots \\ f_1^{(K-1)}(x) & f_2^{(K-1)}(x) & \cdots & f_K^{(k-1)}(x) \end{vmatrix}. \tag{6}$$

The Wronskian test states that, if $W_f(x) \neq 0$ for some x, then the functions are linearly independent [22]–[24].

For the underlying problem, we analyze the Wronskian of the $\tilde{N}$ exponential functions $e^{\jmath p_{\tilde{n}} \tilde{\phi}_l}$ for $\tilde{n} = [1, 2, \cdots, \tilde{N}]$ in the steering vector of the oversampled ULA defined in (5). Taking the derivative of the exponents with respect to

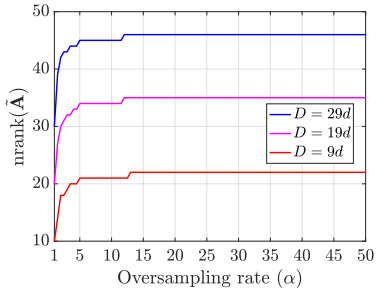

(a) Comparison of numerical rank increment of integer and non-integer arrays.

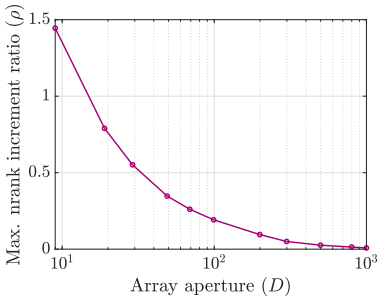

(b) Maximum numerical rank increment ratio approaches to zero for large ULAs

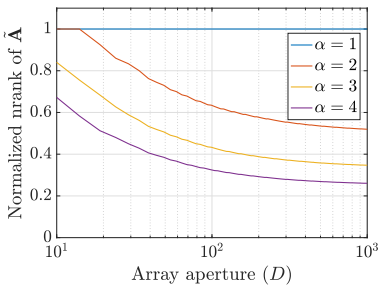

(c) Numerical rank of $\tilde{\mathbf{A}}$ per sensor versus array aperture for different α

Fig. 2: Additional information due to oversampling asymptotically reduces to zero as the ULA becomes larger.

$\sin(\theta_l)$, the Wronskian of the $\tilde{N}$ exponential functions upon simplification using chain rule is given as

$$W = f_{\alpha,\tilde{N}} \cdot \left(\prod_{\tilde{n}=1}^{\tilde{N}} e^{\jmath p_{\tilde{n}} \tilde{\phi}_l} \right) \cdot \begin{vmatrix} w_1^0 & w_2^0 & \cdots & w_{\tilde{N}}^0 \\ w_1 & w_2 & \cdots & w_{\tilde{N}} \\ w_1^2 & w_2^2 & \cdots & w_{\tilde{N}}^2 \\ \vdots & \vdots & \ddots & \vdots \\ w_1^{\tilde{N}-1} & w_2^{\tilde{N}-1} & \cdots & w_{\tilde{N}}^{\tilde{N}-1} \end{vmatrix}, \tag{7}$$

where $f_{\alpha,\tilde{N}} = \alpha^{-\frac{\tilde{N}(\tilde{N}-1)}{2}}$ and $w_{\tilde{n}} = (\jmath 2\pi d p_{\tilde{n}})/\lambda$ with $p_{\tilde{n}} = \tilde{n}-1$. Note that the Vandermonde matrix in (7), i.e., the matrix inside the determinant with basis elements $w_1, w_2, \ldots, w_{\tilde{N}}$, is full rank since its basis elements are all unique, as $p_{\tilde{n}}$ is distinct for all $\tilde{n}$. Therefore, the Vandermonde matrix has a non-zero determinant. Moreover, it is evident that the first and second terms on the right-hand side of (7) are also always non-zero. Therefore, the Wronskian W is always non-zero, indicating that $\tilde{\mathbf{A}}$ is theoretically full rank. □

Using the expression for the determinant of Vandermonde matrices in [25], the absolute value of (7) is obtained as

$$|W| = \alpha^{-\frac{\tilde{N}(\tilde{N}-1)}{2}} \left(\frac{2\pi d}{\lambda}\right)^{\frac{\tilde{N}(\tilde{N}-1)}{2}} \prod_{m=1}^{\tilde{N}-1} m! \,. \tag{8}$$

From (8), we can verify that the Wronskian remains non-zero and $\tilde{\mathbf{A}}$ is theoretically full rank even as $\tilde{N}$ increases.

B. Effect on the Smallest Singular Value due to Oversampling

In this subsection, we examine the numerical rank of $\tilde{\mathbf{A}}$ by deriving an upper bound on its minimum singular value $\mu_{\min}(\tilde{\mathbf{A}})$, and identify the condition for $\mu_{\min}(\tilde{\mathbf{A}})$ to fall below a given threshold, causing the oversampled array manifold to become numerically rank deficient.

The sine values of the DOAs of the L signals impinging on the $\tilde{N}$-element oversampled ULA are selected by uniformly discretizing the interval $[-1, 1]$, corresponding to the sine space of $[-90°, 90°]$, into $L+1$ equidistant points, and discarding the first point at -1. It is noted that, instead of uniformly sample θ, we uniformly discretize $\sin(\theta)$ to ensure equal phase shifts in the resulting array manifold. Thus, for the ith signal, we have $\sin(\theta_i) = -1 + (2i/L)$. Since the array manifold of a ULA is Vandermonde, the basis element corresponding to ith signal is

$$a_i = e^{\jmath \frac{2\pi \tilde{d}}{\lambda} \sin(\theta_i)} = e^{-\jmath \frac{2\pi \tilde{d}}{\lambda}} \cdot e^{\jmath \frac{2\pi \tilde{d}}{\lambda} \frac{2i}{L}}. \tag{9}$$

The determinant of $\tilde{\mathbf{A}}$ in terms of its basis elements is

$$\det(\tilde{\mathbf{A}}) = \prod_{1 \le i < k \le L} e^{-\jmath \frac{2\pi \tilde{d}}{\lambda}} \left(e^{\jmath \frac{2\pi \tilde{d}}{\lambda} \frac{2k}{\tilde{N}}} - e^{\jmath \frac{2\pi \tilde{d}}{\lambda} \frac{2i}{\tilde{N}}} \right). \tag{10}$$

Using $e^{\jmath\theta} - e^{\jmath\phi} = e^{\jmath \frac{\theta+\phi}{2}} \left[e^{\jmath \frac{\theta-\phi}{2}} - e^{-\jmath \frac{\theta-\phi}{2}} \right]$, $e^{\jmath x} - e^{-\jmath x} = 2\jmath \sin(\mathrm{x})$ and, since $L = \tilde{N}$, (10) can be simplified to

$$\det(\tilde{\mathbf{A}}) = \prod_{1 \le k < i \le \tilde{N}} e^{\jmath \frac{2\pi \tilde{d}}{\lambda} \left(\frac{k+i}{\tilde{N}} - 1\right)} \left[2\jmath \sin\left(\frac{2\pi \tilde{d}(k-i)}{\lambda \tilde{N}} \right) \right]. \tag{11}$$

Therefore, the absolute value of the determinant of $\tilde{\mathbf{A}}$ is

$$|\det(\tilde{\mathbf{A}})| = \prod_{1 \le k < i \le \tilde{N}} \left| 2 \sin\left(\frac{2\pi \tilde{d}(k-i)}{\lambda \tilde{N}} \right) \right|. \tag{12}$$

For a particular difference $\Delta = k - i$ which can take values from 1 to $\tilde{N}-1$, there are exactly $\tilde{N} - \Delta$ pairs, i.e., $\tilde{N}-1$ pairs for $\Delta = k-i = 1$, $\tilde{N}-2$ pairs for $\Delta = k-i = 2$, and so on. Thus, (12) can be further simplified as

$$|\det(\tilde{\mathbf{A}})| = \prod_{\Delta=1}^{\tilde{N}-1} \left| 2\sin\left(\frac{\pi \Delta}{\alpha \tilde{N}} \right) \right|^{\tilde{N}-\Delta}. \tag{13}$$

For any square matrix $\tilde{\mathbf{A}}$, the determinant of $\tilde{\mathbf{A}}^{\mathrm{H}}\tilde{\mathbf{A}}$ is $\det(\tilde{\mathbf{A}}^{\mathrm{H}}\tilde{\mathbf{A}}) = |\det(\tilde{\mathbf{A}})|^2$ and, as $\tilde{\mathbf{A}}^{\mathrm{H}}\tilde{\mathbf{A}}$ is Hermitian and positive semi-definite, its smallest eigenvalue is related to the absolute value of its determinant as $\gamma_{\min}(\tilde{\mathbf{A}}^{\mathrm{H}}\tilde{\mathbf{A}}) \le |\det(\tilde{\mathbf{A}}^{\mathrm{H}}\tilde{\mathbf{A}})|^{1/\tilde{N}}$. Moreover, since $\mu_{\min}(\tilde{\mathbf{A}}) = [\gamma_{\min}(\tilde{\mathbf{A}}^{\mathrm{H}}\tilde{\mathbf{A}})]^{1/2}$, by utilizing the result in (13), the smallest singular value of $\tilde{\mathbf{A}}$ is upper bounded by $\mu_{\min}(\tilde{\mathbf{A}}) \le |\det(\tilde{\mathbf{A}})|^{1/\tilde{N}}$, given as

$$\mu_{\min}(\tilde{\mathbf{A}}) \le \prod_{\Delta=1}^{\alpha(N-1)} \left| 2\sin\left(\frac{\pi \Delta}{\alpha^2(N-1)+\alpha} \right) \right|^{1 - \frac{\Delta}{\alpha(N-1)+1}}. \tag{14}$$

As N increases, the sine term in (14) rapidly decreases, allowing the small-angle approximation. As a result, $\mu_{\min}(\tilde{\mathbf{A}})$ is proportional to $\mathcal{O}(\alpha^{-2\alpha(N-1)} N^{-\alpha(N-1)})$, demonstrating exponential decay with respect to both α and N.

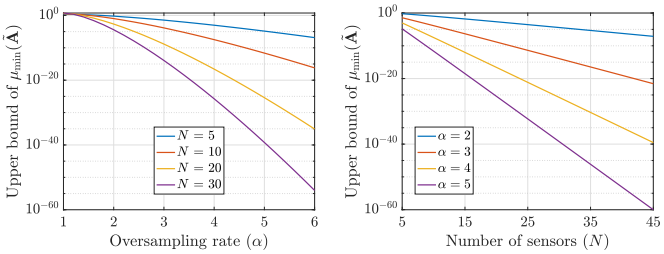

(a) Effect of α on upper-bound of $\mu_{\min}(\tilde{\mathbf{A}})$ for different N (b) Effect of N on upper-bound of $\mu_{\min}(\tilde{\mathbf{A}})$ for different α

Fig. 3: Exponential decay of the upper-bound of $\mu_{\min}(\tilde{\mathbf{A}})$ with oversampling factor and number of sensors.

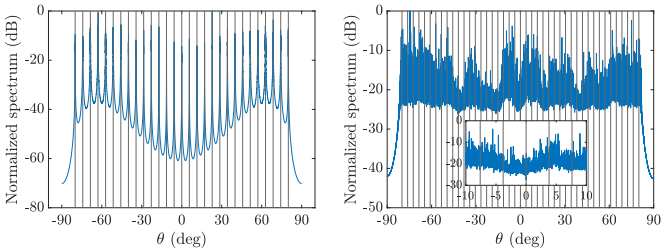

(a) When $\tilde{N} = 30$ all $L = 29$ signals are detected (b) When $\tilde{N} = 44$ all $L = 43$ signals cannot be detected

Fig. 4: Oversampling the ULA with aperture of $D = 19d$ to detect higher number of signals.

It is noted that, in this letter, the identifiability of oversampled ULAs is analyzed through the smallest singular value of $\tilde{\mathbf{A}}$, derived under ideal conditions without accounting for noise or mutual coupling. In practice, the smallest singular value is affected by these factors, which can cause the available DOFs to degrade at lower SNR levels.

IV. Numerical Results

In this section, we present simulation results that support our findings in Section III and illustrate the impact of N and α on the numerical rank of $\tilde{\mathbf{A}}$. The numerical rank of $\tilde{\mathbf{A}}$, denoted as $\mathrm{nrank}(\tilde{\mathbf{A}})$, is given as the number of singular values of $\tilde{\mathbf{A}}$ that are above a specified threshold μ_{thr}. In the numerical evaluations, we consider $\mu_{\mathrm{thr}} = 10^{-6}$.

Fig. 2(a) illustrates how the numerical rank of the array manifold varies as ULAs of different apertures are oversampled. 10-, 20- and 30-element ULAs are respectively considered. In all the cases the oversampling rate is increased while keeping the aperture fixed. Note that for all three ULAs, the numerical rank initially increases linearly with oversampling, reaching $\mathrm{nrank}(\tilde{\mathbf{A}}) = \tilde{N}$. However, beyond a certain level of oversampling, the smallest singular value falls below the threshold and $\tilde{\mathbf{A}}$ is no longer numerically full rank. For the ULA with aperture $9d$, $\mathrm{nrank}(\tilde{\mathbf{A}})$ stabilizes at 22 as oversampling increases. Similarly, for ULAs with aperture $19d$ and $29d$, the numerical rank stabilizes at 34 and 45, respectively.

To quantify the rank increment of $\tilde{\mathbf{A}}$ due to spatial oversampling, we define the maximum rank increment ratio (ρ) as the ratio of the maximal rank gain, achieved by oversampling an N-element ULA, to its aperture. Considering an N-element ULA with an aperture of $D = (N-1)d$, ρ is given as

$$\rho = \frac{\max \mathrm{nrank}(\tilde{\mathbf{A}}) - \mathrm{nrank}(\mathbf{A})}{N-1}. \tag{15}$$

For example, for the 10-element ULA results shown in Fig. 2(a), as $\max \mathrm{nrank}(\tilde{\mathbf{A}}) = 22$, we obtain $\rho = (22-9)/9 \approx 1.44$. Fig. 2(b) depicts how the maximum rank increment ratio varies with the ULA aperture. It reveals that, as the ULA aperture or, equivalently, the number of sensors N increases, the numerical rank gain from oversampling gradually decreases and eventually converges to zero. In other words, the marginal increase in DOFs due to oversampling decreases with aperture growth and vanishes asymptotically as $N \to \infty$.

Fig. 2(c) illustrates the normalized $\mathrm{nrank}(\tilde{\mathbf{A}})$, defined as $\mathrm{nrank}(\tilde{\mathbf{A}})/\tilde{N}$, plotted against the array aperture D for different oversampling factors α. It is observed that, for $\alpha = 1$, the ratio remains 1, indicating that all sensors contribute to the numerical rank of $\tilde{\mathbf{A}}$. However, for $\alpha > 1$, the ratio decreases with increasing array aperture, indicating that not all sensors in the oversampled ULA contribute to the numerical rank. Specifically, for $\alpha = 2, 3$ and 4, the normalized numerical rank asymptotically approaches $1/2, 1/3$ and $1/4$ respectively. This implies that, in the limit of an infinitely large ULA, only a fraction $1/\alpha$ of the $\tilde{N}$ sensors contribute to the numerical rank of $\tilde{\mathbf{A}}$. Therefore, for asymptotically large ULAs, oversampling no longer offers advantages in terms of numerical rank.

Figs. 3(a) and 3(b) show the upper bound of the smallest singular value of $\tilde{\mathbf{A}}$, as given in (14), versus α and N. As seen earlier in Fig. 2(a), $\tilde{\mathbf{A}}$ initially retains full numerical rank underspatial oversampling, but becomes rank-deficient when $\mu_{\min}(\tilde{\mathbf{A}})$ drops below the critical threshold which depends on N. Once this threshold is crossed and a DOF is lost, $\mathrm{nrank}(\tilde{\mathbf{A}})$ quickly saturates despite further oversampling.

Fig. 4 illustrates the DOA estimation performance for an oversampled ULA. In Fig. 4(a), a ULA with aperture of $D = 19d$ oversampled with $\tilde{N} = 30$ sensors, can successfully detect $L = 29$ signals uniformly distributed over the angular range of $[-80°, 80°]$. However, as shown in Fig. 4(b), when the same aperture is oversampled using $\tilde{N} = 44$ sensors, the array fails to identify $L = 43$ signals uniformly distributed over the same angular range. This result confirms our analysis that, for a 20-element ULA with an aperture of $19d$, the maximum numerical rank of $\tilde{\mathbf{A}}$ saturates at 34 for large $\tilde{N}$, as shown in Fig. 2(a).

V. Conclusion

In this letter, we investigated the impact of spatial oversampling on the identifiability of a ULA. Although the array manifold of an oversampled ULA with finite aperture is theoretically full rank, we showed it may become numerically rank-deficient. We analyzed the effective DOFs via the numerical rank and derived an upper bound on the smallest singular value of the array manifold. Our analysis delineates the conditions under which spatial oversampling yields meaningful benefits and where such gains diminish, offering insights into the interplay among spatial oversampling, array aperture, and signal identifiability.

REFERENCES

[1] D. H. Johnson, *Array Signal Processing: Concepts and Techniques*. Prentice-Hall, 1993.

[2] H. L. Van Trees, *Optimum Array Processing: Part IV of Detection, Estimation, and Modulation Theory*. Wiley, 2002.

[3] T. E. Tuncer and B. Friedlander, *Classical and Modern Direction-of-Arrival Estimation*. Academic Press, 2009.

[4] X. Zhang, L. Xu, L. Xu, and D. Xu, "Direction of departure (DOD) and direction of arrival (DOA) estimation in MIMO radar with reduced-dimension MUSIC," *IEEE Comm. Lett.*, vol. 14, no. 12, pp. 1161–1163, 2010.

[5] A. Hassanien and S. A. Vorobyov, "Transmit energy focusing for DOA estimation in MIMO radar with colocated antennas," *IEEE Trans. Signal Process.*, vol. 59, no. 6, pp. 2669–2682, 2011.

[6] S. Sun and Y. D. Zhang, "4D automotive radar sensing for autonomous vehicles: A sparsity-oriented approach," *IEEE J. Sel. Topics Signal Process.*, vol. 15, no. 4, pp. 879–891, 2021.

[7] C. Zhou, Y. Gu, Y. D. Zhang, and Z. Shi, "Sparse array interpolation for direction-of-arrival estimation," in *Sparse Arrays for Radar, Sonar, and Communications*, M. G. Amin, Ed. Wiley-IEEE Press, 2024.

[8] P. Kulkarni and P. Vaidyanathan, "Non-integer arrays for array signal processing," *IEEE Trans. Signal Process.*, vol. 70, pp. 5457–5472, 2022.

[9] ——, "Rational arrays for DOA estimation," in *Proc. IEEE Int. Conf. Acoust., Speech Signal Process. (ICASSP)*, 2022, pp. 5008–5012.

[10] Y. D. Zhang, M. G. Amin, F. Ahmad, and B. Himed, "DOA estimation using a sparse uniform linear array with two CW signals of co-prime frequencies," in *Proc. IEEE Int. Workshop Comput. Adv. Multi-Sensor Adapt. Process. (CAMSAP)*, 2013, pp. 404–407.

[11] E. BouDaher, Y. Jia, F. Ahmad, and M. G. Amin, "Multi-frequency co-prime arrays for high-resolution direction-of-arrival estimation," *IEEE Trans. Signal Process.*, vol. 63, no. 14, pp. 3797–3808, 2015.

[12] S. Qin, Y. D. Z. M. G. Amin, and B. Himed, "DOA estimation exploiting a uniform linear array with multiple co-prime frequencies," *Signal Process.*, vol. 130, pp. 37–46, 2017.

[13] S. Zhang, A. Ahmed, Y. D. Zhang, and S. Sun, "Enhanced DOA estimation exploiting multi-frequency sparse array," *IEEE Trans. Signal Process.*, vol. 69, pp. 5935–5946, 2021.

[14] Y. D. Zhang and M. G. Amin, "Multi-frequency rational sparse array for direction-of-arrival estimation," in *Proc. Int. Symp. Signals Circuits Syst. (ISSCS)*, 2023, pp. 1–4.

[15] M. W. T. S. Chowdhury and Y. D. Zhang, "Unambiguous DOA estimation using multi-frequency rational sparse arrays," in *Proc. Asilomar Conf. Signals Syst. Comput.*, 2023, pp. 1324–1328.

[16] M. W. T. S. Chowdhury, Y. D. Zhang, W. Liu, and M. S. Greco, "Identifiability analysis of sensor arrays with sensors off half-wavelength grid," in *Proc. IEEE Int. Conf. Acoust., Speech Signal Process. (ICASSP)*, 2024, pp. 8496–8500.

[17] M. W. T. S. Chowdhury, Y. D. Zhang, and B. Himed, "Identifiability analysis of non-integer antenna arrays in the presence of mixed (strong and weak) signals," in *Proc. Int. Radar Conf.*, 2024, pp. 1–6.

[18] C. Huang, S. Hu, G. C. Alexandropoulos, A. Zappone, C. Yuen, R. Zhang, M. Di Renzo, and M. Debbah, "Holographic MIMO surfaces for 6G wireless networks: Opportunities, challenges, and trends," *IEEE Wireless Commun.*, vol. 27, no. 5, pp. 118–125, 2020.

[19] T. Gong, P. Gavriilidis, R. Ji, C. Huang, G. C. Alexandropoulos, L. Wei, Z. Zhang, M. Debbah, H. V. Poor, and C. Yuen, "Holographic MIMO communications: Theoretical foundations, enabling technologies, and future directions," *IEEE Commun. Surv. Tutorials*, 2023.

[20] L. Wei, C. Huang, G. C. Alexandropoulos, E. Wei, Z. Zhang, M. Debbah, and C. Yuen, "Multi-user holographic MIMO surfaces: Channel modeling and spectral efficiency analysis," *IEEE J. Sel. Topics Signal Process.*, vol. 16, no. 5, pp. 1112–1124, 2022.

[21] A. Pizzo, T. L. Marzetta, and L. Sanguinetti, "Spatially-stationary model for holographic MIMO small-scale fading," *IEEE J. Sel. Areas Commun.*, vol. 38, no. 9, pp. 1964–1979, 2020.

[22] A. Bostan and P. Dumas, "Wronskians and linear independence," *American Math. Monthly*, vol. 117, no. 8, pp. 722–727, 2010.

[23] A. Garcia and J. F. Voloch, "Wronskians and linear independence in fields of prime characteristic," *Manuscripta Math.*, vol. 59, no. 4, pp. 457–469, 1987.

[24] K. Wolsson, "A condition equivalent to linear dependence for functions with vanishing Wronskian," *Linear Algebra Appl.*, vol. 116, pp. 1–8, 1989.

[25] K. Lundengård, J. Österberg, and S. Silvestrov, "Optimization of the determinant of the vandermonde matrix and related matrices," *Methodol. Comput. Appl. Probab.*, vol. 20, no. 4, pp. 1417–1428, 2018.